scientific reports

Check for updates

OPEN

Phosphotyrosine proteomics reveals novel Zap70 and Itk pathway targets downstream of TCR and CAR in Jurkat T cells

Aurora Callahan, Savannah S. Trychanh, Timothy Ro, Aisharja Mojumdar & Arthur R. Salomon✉

Z-associated protein of 70 kDa (Zap70) and interleukin-2-inducible T cell kinase (Itk) propagate the primary and CD28-integrated phosphotyrosine (pY) signalling, respectively, to achieve full T cell activation. Despite their canonical roles in T cell activation, our understanding of how each kinase controls canonical and noncanonical pY signalling is incomplete. Here, using three T cell activation methods (soluble antibodies, APC-pMHC/TCR, and CD19-CAR/Raji), we evaluated the effects of two novel inhibitors, RDN2150 (RDN, Zap70) and Soquelitinib (Soq, Itk), on T cell activation. We validated the published working concentrations of RDN and Soq on phosphorylation of key T cell signalling proteins and on T cell activation markers, finding that RDN provides more complete inhibition of T cell signalling and activation. We used LC–MS/MS to evaluate how RDN and Soq treatment affected the phosphotyrosine (pY) signalling and proteome of T cells, finding that RDN, as opposed to Soq, completely downregulated the TCR signalling pathway. Finally, we identified new, noncanonical pY sites responsive to RDN and Soq, providing new insights into the pathways regulated by Zap70 and Itk. Together, our work provides a basis for further study on RDN and Soq, as well as a molecular roadmap for the effects of these inhibitors.

Keywords Itk, Chimeric antigen receptor, Soquelitinib, Zap70, RDN2150, Phosphotyrosine proteomics

T cell activation through the T cell receptor (TCR) is initiated by binding of a peptide-presenting major histocompatibility complex (pMHC) on an antigen-presenting cell. It requires the coordinated activity of tyrosine kinases, including the Src family kinase Leukocyte C-terminal Src kinase (Lck), the Syk family kinase ζ-associated protein of 70 kDa (Zap70), and the Tec family kinase interleukin 2 inducible T cell kinase (Itk)[1]. TCR-pMHC ligation promotes Lck^{Y505} dephosphorylation by CD45 and subsequent Lck^{Y394} autophosphorylation and phosphorylation of immunoreceptor tyrosine-based activation motifs (ITAMs) on TCR subunits CD3ϵ, CD3γ, CD3δ, and TCRζ, which Zap70 is then able to bind through its dual SH2 domains. Lck activates Zap70 and Itk through phosphorylation at $Zap70^{Y493}$ and Itk^{Y512}, respectively, and linker for activation of T cells (LAT), a scaffolding protein necessary for TCR signalling, is activated by Lck-mediated Zap70 phosphorylation at multiple tyrosine residues. Multiple scaffolding proteins, including SLP76-bound GADS and phospholipase C γ1 (PLCγ1), dock on LAT, allowing for the phase separation of the TCR signalosome and bringing substrates into proximity with Lck, Zap70, and Itk for phosphorylation and activation. Components of the TCR signalosome then propagate signal to reorganise the actin cytoskeleton and activate transcription factors, promoting T cell activation and feedback regulation of the signalling input (reviewed extensively in Gaud et al. 2018). Notably, mutations to Zap70 are associated with autoimmune disorders and loss of Zap70 ablates T cell activation, while inhibition of Itk alters the fate of T cells and is associated with better prognosis in immunotherapeutic intervention in various diseases[2,3].

Chimeric antigen receptors (CARs), a novel immunotherapy for the treatment of autoimmune disorders and cancers, are composed of domains from T cell signalling proteins, with the goal of engaging a disease-associated antigen and initiating an immune response[4,5]. Clinically available CAR designs include the intracellular domain of TCRζ and costimulation via the intracellular domain of either CD28 or 4-1BB, two T cell costimulatory receptors that enhance T cell activation and memory T cell formation, respectively[6,7]. Despite hundreds of clinical trials evaluating the safety and efficacy of CARs in humans, only six are currently approved for use as a

Department of Molecular Biology, Cell Biology, and Biochemistry, Brown University, Providence, RI 02903, USA. ✉email: art@drsalomon.com

last resort for relapsed or refractory cancers of blood cell lineage[6]. CAR T cell therapy is often plagued by non-specific T cell activation, low antigen sensitivity, and T cell exhaustion, leading to variable patient responses, at worst resulting in no tumour clearance, cytokine release syndrome, and neurotoxicity resulting from enhanced immune activity in the brain[8]. Recent literature suggests that altered T cell activation is the result of aberrant engagement of the TCR signalling pathway, including constitutive docking of active Lck on CD28 costimulated CARs, a lack of recruitment of key TCR signalling proteins after antigen ligation on 4-1BB costimulated CARs, and differential engagement with the TCR signalosome[9–11]. Researchers have demonstrated that disrupting the Itk binding site in the CD28 costimulatory domain (PRRP to ARRA) or the GADS binding site (YMNM to FMNM) can significantly enhance the function of second-generation CARs with a CD28 domain, thereby reducing constitutive, continuous CAR activation[12,13]. Currently, efforts to restrain CAR-induced toxicities have come from high-throughput Jurkat screens evaluating combinatorial CAR libraries for sustained T cell activation with low exhaustion markers, and from the rational design of new CARs, including dual-antigen split CARs and "fourth-generation CARs," known as T cells redirected for universal cytokine-mediated killing (TRUCKs)[14–21]. Even with advances in the functional understanding of CAR T cells, basic research evaluating how CARs influence T cell biology, particularly T cell activation, is lagging.

Two small-molecule inhibitors with distinct effects on T-cell signalling have recently been described: RDN2150 (RDN) targeting Zap70 and Soquelitinib (Soq) targeting Itk[22,23]. RDN covalently inhibits Zap70 and prevents phosphorylation of LAT^{Y220}, thereby destabilising the LAT/SLP76 complex. At concentrations less than 400 nM, RDN reduces interferon-γ and interleukin-17A, and is effective in treating psoriasis in murine models by topical application[22]. Soq is a highly selective covalent inhibitor of Itk, thought to reduce phosphorylation of PLCγ1^{Y783} and thus reduce T cell activation strength[23]. In this paper, we provide a thorough evaluation of RDN and Soq in the context of Jurkat signalling and activation. By performing inhibitor treatments across three distinct models of T cell activation (soluble antibody crosslinking, APC-pMHC/TCR co-culture, and CD19-CAR/Raji co-culture), we find that RDN's efficacy in abating T or CAR T cell signalling is higher than its efficacy in disrupting T cell activation markers. Further, Soq appears to thoroughly disrupt PLCγ1^{Y783} phosphorylation and IL-2 production even at low concentrations, while leaving CD69 expression intact. Finally, we find that while soluble antibody stimulation induces the most pY induction of any stimulation method, it is unable to activate T cells to the same degree as APC-pMHC/TCR or CD19-CAR/Raji stimulation. Thus, we provide the first phosphoproteomic analysis of RDN and Soq in the context of T and CAR T cell signalling and activation, thereby providing a molecular basis for their in vivo effects.

Results

Soq inhibits PLCγ1 phosphorylation without large-scale disturbance of the TCR signalling pathway

Given the novelty and potential therapeutic applications of RDN and Soq, we aimed to thoroughly characterise their effects on Jurkat T- and CAR T cell signalling and activation (Fig. 1A). Despite genomic instability among Jurkat lines across research groups[24], these lines enable large-scale, deep phosphoproteomic analysis that has shaped the field of T cell signalling[25]. We performed a titration of RDN and Soq on Jurkat T cells and assessed phosphorylation of key TCR signalling proteins after T cell activation by soluble antibody stimulation of the TCR and CD28, APC-pMHC/TCR co-culture, and CD19-CD28-ζ CAR/Raji (CD19-CAR/Raji) co-culture. We showed that our Jurkat T cell sublines (J^{OT1} and CD19-CAR Jurkats) are distinguishable by GFP expression and retain high surface expression of CD45, CD28, CD3ε, and TCRαβ (Supporting Fig. 1A–E). Further, T2-Kb cells (used as APCs for J^{OT1} cells) and Raji cells highly express CD45, CD80, and CD86 (Supporting Fig. 1F–H). We demonstrated that low concentrations (100 nM) of RDN or Soq were sufficient to reduce basal Erk1/2 phosphorylation (Supporting Fig. 2). We found that only 10 μM RDN was sufficient to impair phosphorylation of LAT^{Y220}, a direct substrate of Zap70[26] (Fig. 1B–D). Phosphorylation of Lck^{Y394} was unaffected by RDN (Fig. 1B, Supporting Fig. 3), but the downstream pathway targets Erk1^{T202Y204}/Erk2^{T185Y187} were significantly reduced at 1 and 10 μM RDN after 2.5 min of stimulation. During soluble antibody stimulation, Soq treatment did not significantly disrupt PLCγ1^{Y783} phosphorylation, a direct substrate of Itk, after 2.5 min. It minimally affected Erk1^{T202Y204}/Erk2^{T185Y187} until a concentration of 10 μM Soq and did not affect LAT^{Y220} or Lck^{Y394} (Fig. 1B–D, Supporting Fig. 3). These trends remained true irrespective of the method of stimulation (Fig. 1E–J, Supporting Figs. 4, 5), except for PLCγ1^{Y783}, which was significantly impaired after Soq treatment in APC-pMHC/TCR and CD19-CAR/Raji conditions. Lck^{Y394} was not induced during APC-pMHC/TCR or CD19-CAR/Raji co-cultures (Supporting Figs. 4 and 5). We also observed that phosphorylation of early TCR signalling proteins peaked approximately 2.5 min after stimulation, with a subsequent decline by 10 min (Fig. 1, Supporting Figs. 3–5, Supporting Tables 1–12). Importantly, CD19-CAR Jurkats maintain high induction of phosphorylation in response to soluble antibody stimulation (Supporting Fig. 6), thus low induction during CAR/Raji co-culture is not due to general signalling incompetence in CD19-CAR Jurkats. These data suggest that 10 μM RDN is required to disrupt phosphorylation-based TCR/CAR signalling, whereas 10 μM Soq or higher is required to achieve maximal Itk inhibition.

Both RDN and Soq inhibit IL-2 expression, but only RDN blocks CD69 upregulation

Signalling from the TCR/CAR is a rapid process, leading to the expression of new genes and the presentation/release of new proteins that elicit intercellular effects, such as cell death or the activation of neighbouring immune cells. T cell activation is a finely tuned process that requires precise, time-dependent activation of each component of the signalling pathway, and small perturbations can lead to over- or under-activation of T cells, ultimately resulting in autoimmunity[27]. To determine whether RDN or Soq impacted overall T cell activation, we evaluated expression of CD69 and IL-2, two activation markers of T and CAR T cells, after 24 h of antibody-, pMHC-, and CD19-CAR/Raji-induced T cell activation. We found that soluble antibody stimulation mildly

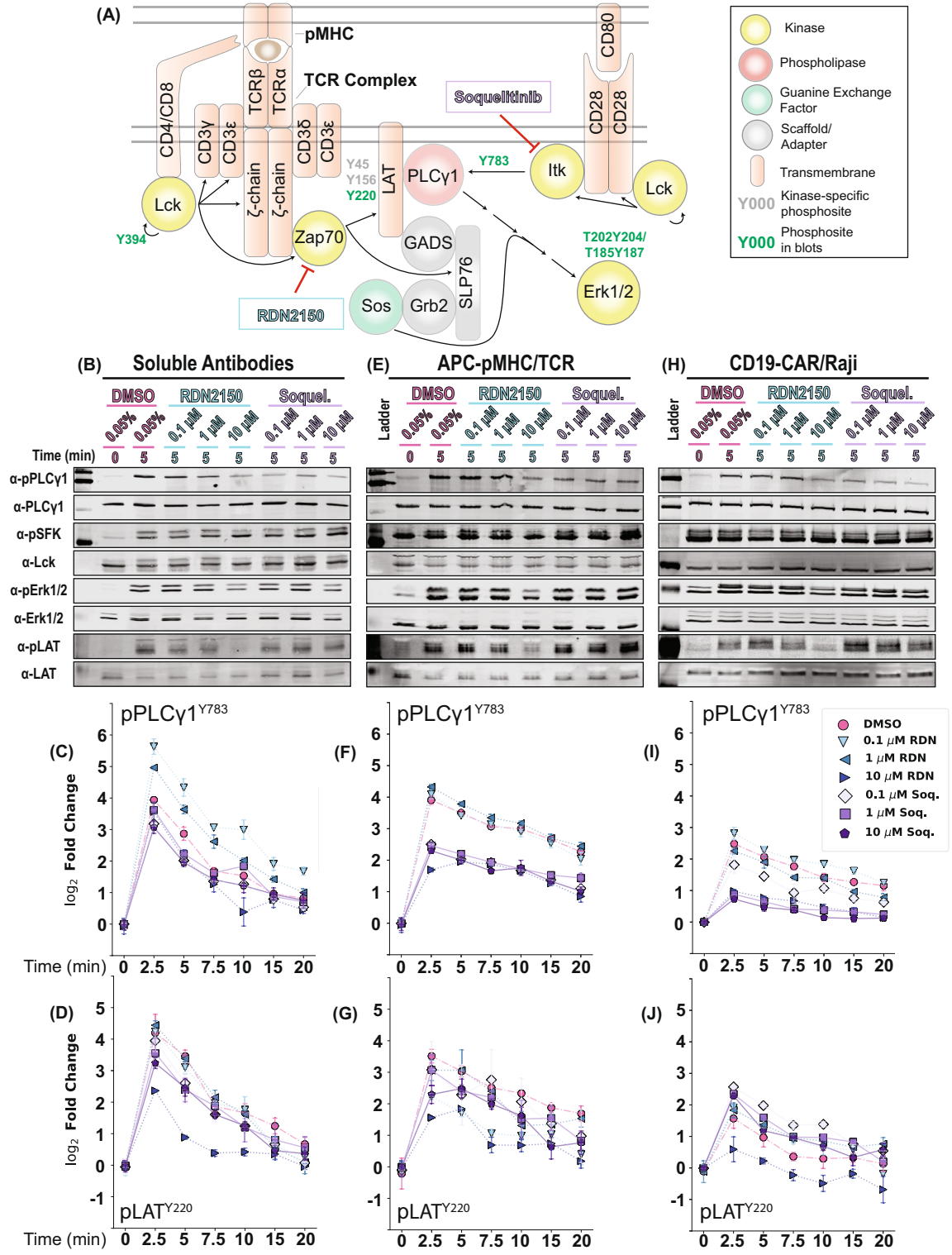

Fig. 1. Soq inhibits PLCγ1^{Y783} while RDN inhibits both PLCγ1^{Y783} and LAT^{Y220} phosphorylation. (**A**) Schematic representation of T cell signalling, indicating the expected effects of inhibiting Zap70 (RDN) or Itk (Soq). Phosphorylation sites depicted in green are probed in subsequent Western blots. (**B**) Representative Western blots targeting PLCγ1^{Y783}/PLCγ1, SFK^{Y416}/Lck, Erk1^{T202Y204}/Erk1 and Erk2^{T185Y187}/Erk2, and LAT^{Y220}/LAT in soluble antibody stimulation of the TCR (**C**) Quantification of PLCγ1^{Y783} during a time course soluble antibody stimulation of the TCR. (**D**) Quantification of LAT^{Y220} during a time course soluble antibody stimulation of the TCR. (**E**–**G**) As in (**B**–**D**), except for APC-pMHC stimulation of the Jurkat^{OT-I} TCR. (**H**–**J**) As in (**B**–**D**), except for Raji co-culture stimulation of a second-generation CD19-CAR. Statistical analysis for Western blots was performed using the Holm-Sidak correction of Fisher's LSD pairwise comparisons and is available in Supporting Tables 1, 2, 5, 6, 9, and 10. $n \geq 3$ independent experiments per treatment group/time point.

induced CD69 expression but failed to induce IL-2 expression (Fig. 2A,B, Supporting Tables 13, 14)[28]. These data are consistent with the literature showing that complete T cell activation requires mechanical forces and that clustering of TCR/CD28-bound antibodies using beads or tethering TCR/CD28 antibodies to a surface is necessary for antibody-based T cell activation[29–32]. Treatment with either RDN or Soq significantly reduced soluble antibody stimulation-induced CD69 expression at all tested concentrations (Supporting Table 13), but only 10 μM RDN completely ablated CD69 induction (Fig. 2A). After APC-pMHC/TCR stimulation, CD69 and IL-2 were highly upregulated and significantly reduced after treatment with RDN (Fig. 2C,D). CD69 expression was not affected by any tested concentration of Soq, but Soq treatment significantly reduced IL-2 production after APC-pMHC/TCR stimulation (Fig. 2C,D, Supporting Tables 15, 16). These trends were most evident in CD19-CAR/Raji stimulation conditions, as CD69 was widely expressed after co-culture and was reduced only by RDN treatment. IL-2 production was highest in CAR T cells (~ 1000 pg/mL in DMSO control samples) and was significantly reduced with both RDN and Soq treatment (Fig. 2E,F, Supporting Tables 17, 18). These data in the context of the known TCR pathway ordering confirm that soluble antibody stimulation is insufficient to induce full T cell activation and support that the Itk-mediated branch of TCR signalling is responsible for IL-2 production.

RDN treatment reduces ligand-induced pY signalling more than Soq

To gain precise information regarding the roles of Zap70 and Itk in TCR- and CAR-mediated T cell activation, we leveraged the sensitivity of LC–MS/MS coupled with pY enrichment using the Src SH2 superbinder (sSH2) as previously described[33–37]. We identified a total of 773 T cell-specific pY sites in antibody-stimulated samples with high reproducibility ($R > 0.8$ by multiple regression; see https://github.com/Aurdeegz/Zap70-Itk-Inhibitor-Profiling). Phosphotyrosine signalling from the TCR/CAR is well characterised, and Zap70/Itk have canonical roles in the progression of T cell activation (Fig. 1A)[1,9,10,36,38–40]. Using our pY proteomics data, we observed that 2.5 min of soluble antibody stimulation of the TCR induced large-scale pY induction irrespective of RDN or Soq treatment (Fig. 3A, top row, Supporting Fig. 7). Known components of the TCR signalling cascade, including ITAMs on CD3ε and TCRζ, LAT^{Y220}, Erk2^{T185Y187}, Nck^{Y105}, PLCγ1^{Y775}, PLCγ1^{Y783}, SFK^{Y416}, and Zap70^{Y492} were increased after 2.5 min with or without RDN and Soq. After 10 min, some of these pY sites returned to basal, although some pY sites, including ITAMs, Erk1^{T202Y204}/Erk2^{T185Y187}, PLCγ1^{Y775}, and PLCγ1^{Y783}, remained elevated in DMSO and/or RDN treatment conditions, in line with our titration data (Figs. 1, 3B, Supporting Table 19). Analysis of time course data using post-translational modification signature enrichment analysis (PTM-SEA), a GSEA-like algorithm for PTM proteomics data[41], showed that soluble antibody stimulation strongly engaged TCR signalling kinases (Supporting Fig. 8A), components of various signalling pathways (Supporting Fig. 8B), and Perturbation Signatures associated with cell activation (Supporting Fig. 8C). In contrast, APC-pMHC/TCR stimulation modestly induced pY signalling by Western blot and proteomics for pY, pLAT, and pPLCγ1 (Fig. 3A, middle row, Supporting Fig. 9). The effects of RDN treatment were more evident with fewer significantly induced pY sites after 2.5 min (365 total pY sites, Fig. 3A, middle row). APC-pMHC/TCR stimulation did not uniformly induce phosphorylation along CD3/TCRζ ITAMs, and Soq treatment did very little to reduce pY induction along the T cell signalling pathway (Fig. 3C, Supporting Table 20). In agreement with the antibody stimulation data, APC-pMHC/TCR stimulation significantly upregulated Kinase Signatures (Supporting Fig. 10A), Pathway Signatures with the notable exception of TCR signalling (Supporting Fig. 10B), and perturbation signatures associated with cell activation, including 'ANTI CD3' and 'IL 2' (Supporting Fig. 10C). Interestingly, CD19-CAR/Raji co-culture significantly increased few pY sites (299 total pY sites, Fig. 3A, Supporting Fig. 11) after 2.5 min with TCR signalling pY sites like Erk2^{T185Y187}, Nck1^{Y105}, PLCγ1^{Y775}, PLCγ1^{Y783}, and Zap70^{Y492} being among them in the DMSO control (Fig. 3D, Supporting Table 21). Treatment with RDN ablated the induction of all TCR signalling pY sites at 2.5 min after co-culture. In contrast, Soq treatment had little effect on pY induction along the TCR signalling pathway (Fig. 3D). Finally, although many Kinase Signatures (Supporting Fig. 12A), Pathway Signatures (Supporting Fig. 12B), and Perturbation Signatures (Supporting Fig. 12C) were significantly upregulated in CD19-CAR/Raji stimulations with DMSO or Soq treatment, almost no signatures were significantly induced during RDN treatment, supporting that Zap70 is integral to the CD19-CAR activation[42,43]. These data, in combination with Fig. 1, support the notion that pY induction is heavily dependent on the form of stimulation, and that the effectiveness of RDN and Soq treatment on pY signalling varies greatly with stimulation strength.

RDN treatment disrupts the TCR pathway more than Soq treatment

Given the ability to retain signalling capacity in the presence of each inhibitor, we sought to evaluate how inhibition affected pY-site abundance relative to the DMSO control. As expected, treatment with either 10 μM RDN or 10 μM Soq uniformly reduced pY abundance in soluble antibody-treated samples, with the majority of pY sites being significantly reduced at 0, 2.5, and 10 min of stimulation when compared to the DMSO control (Fig. 4A, Supporting Fig. 7, Supporting Table 19). pY sites along the TCR signalling pathway, including the Erk1/2 activation sites, Jnk2/3 activation sites, and multiple sites on PLCγ1 and Zap70 were reduced during RDN treatment. Interestingly, 10 μM RDN treatment increased Zap70^{Y493} abundance at the basal and 10-min stimulation time points, whereas it reduced various TCR ITAM sites, such as TCRζ^{Y64}/TCRζ^{Y72} and CD3ε^{Y188} (Fig. 4B, Supporting Table 19). PTM-SEA showed downregulation of activating perturbation signatures like 'ANTI CD3' and 'IL 2' (Fig. 4C), and upregulation of inhibitor signatures like 'ERLOTINIB' and 'U0126' (Fig. 4D), suggesting that the phosphoproteomic signature of RDN and Soq mimicked that of pre-established inhibitors. Our results for RDN treatment in APC-pMHC/TCR and CD19-CAR/Raji stimulations were similar, showing that the majority of significantly changing pY sites were reduced (Supporting Figs. 13A, 14A), those sites often were located on TCR signalling pathway proteins (Supporting Figs. 13B, 14B), and that the PhosphositePlus Perturbation signatures and NetPath Pathway signatures were, in general, significantly downregulated during

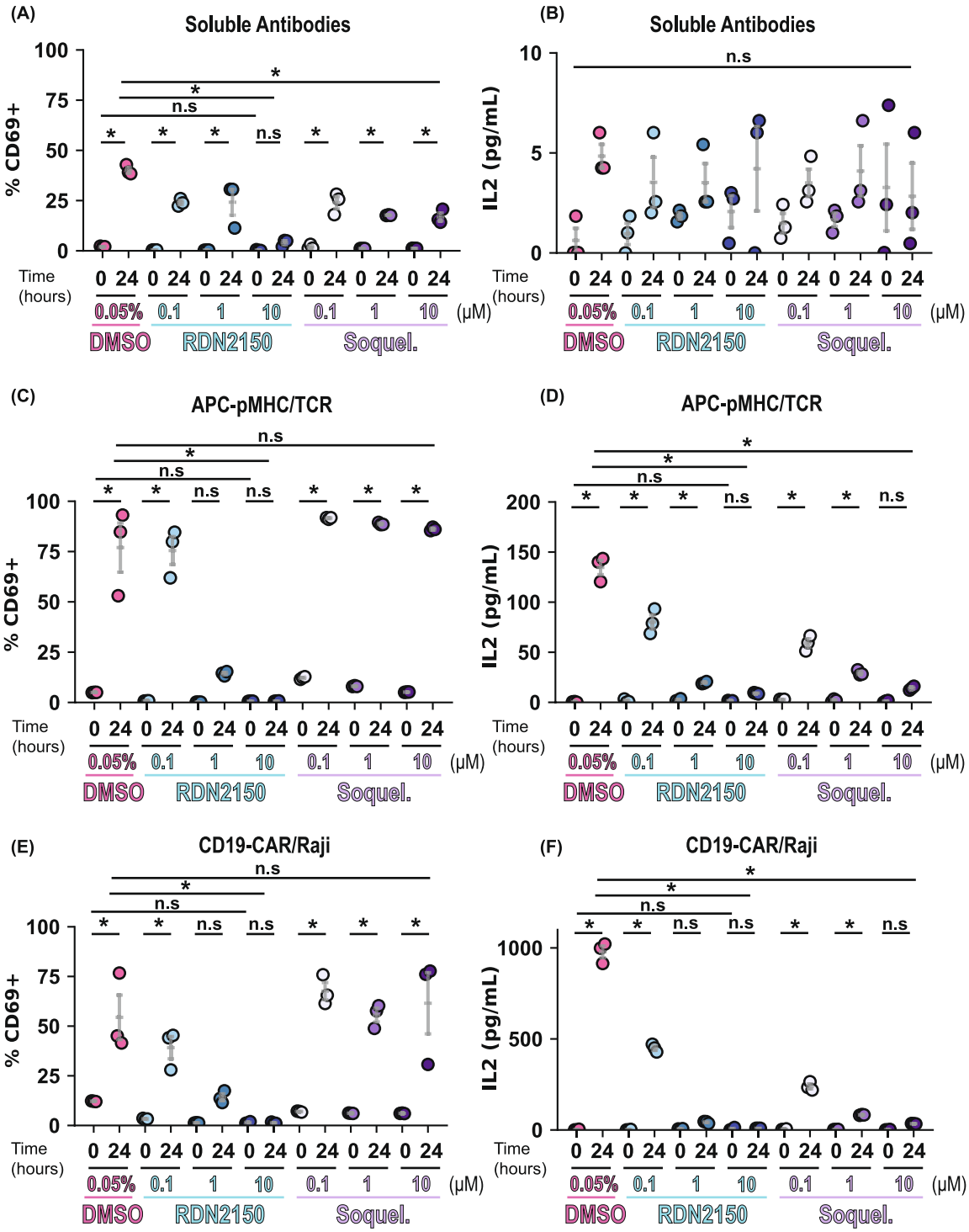

Fig. 2. Interleukin-2 secretion, but not CD69 expression, is significantly reduced by Soq treatment. (**A**) Dotplot showing the percentage of CD69-positive cells measured by flow cytometry after 24 h of soluble antibody stimulation. (**B**) Dotplot showing the concentration of IL-2 in the cell culture supernatant measured by ELISA after 24 h of soluble antibody stimulation. (**C**, **D**) As in (**A**, **B**), except for APC-pMHC stimulation. (**E**–**F**) As in (**A**, **B**), except for Raji-co-culture stimulation of a second-generation CD19-CAR. Statistical analysis for flow cytometry and ELISA data was performed using a one-way ANOVA followed by the Holm-Sidak correction of Fisher's LSD pairwise comparisons, if applicable, and is available in Supporting Tables 13–18. $n = 3$ independent experiments per treatment group.

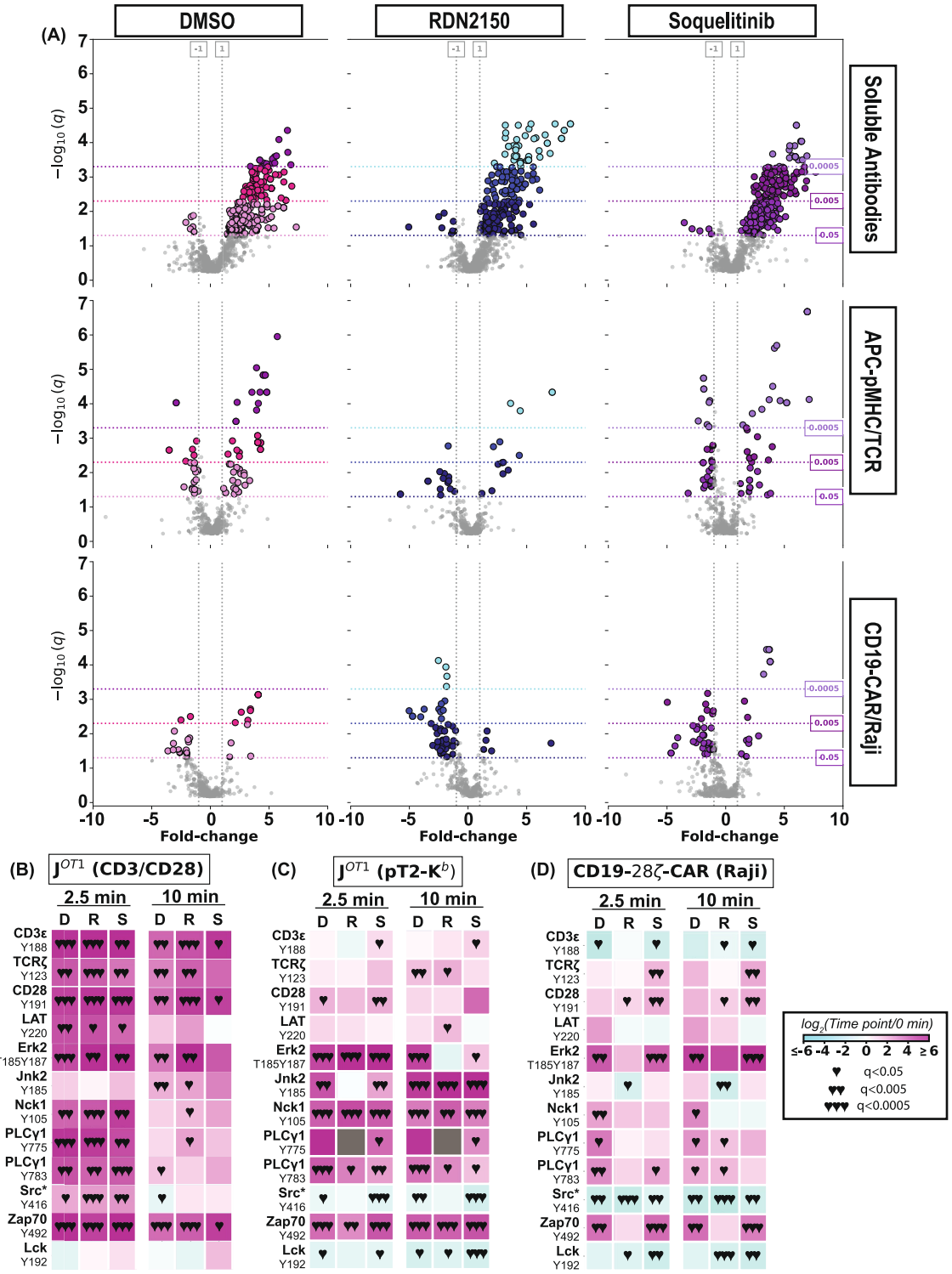

Fig. 3. Antibody/TCR stimulation strongly induces tyrosine phosphorylation irrespective of RDN or Soq treatment. (**A**) Volcano plot analysis of pY proteomics data comparing 2.5 min versus 0 min of antibody stimulation (top), APC-pMHC/TCR stimulation (middle), and CD19-CAR/Raji stimulation (bottom) in DMSO (left), RDN (middle), and Soq (right) treatment conditions. (**B**, **D**) Select site-specific heatmaps of time course pY proteomics data after antibody stimulation, APC-pMHC/TCR stimulation, and CD19-CAR/Raji stimulation. ♥ indicates $q < 0.05$, and ♥♥ indicates $q < 0.005$, and ♥♥♥ indicates $q < 0.0005$. $n \geq 3$ measurements from independent experiments for each unique pY site per treatment group/time point/stimulation method.

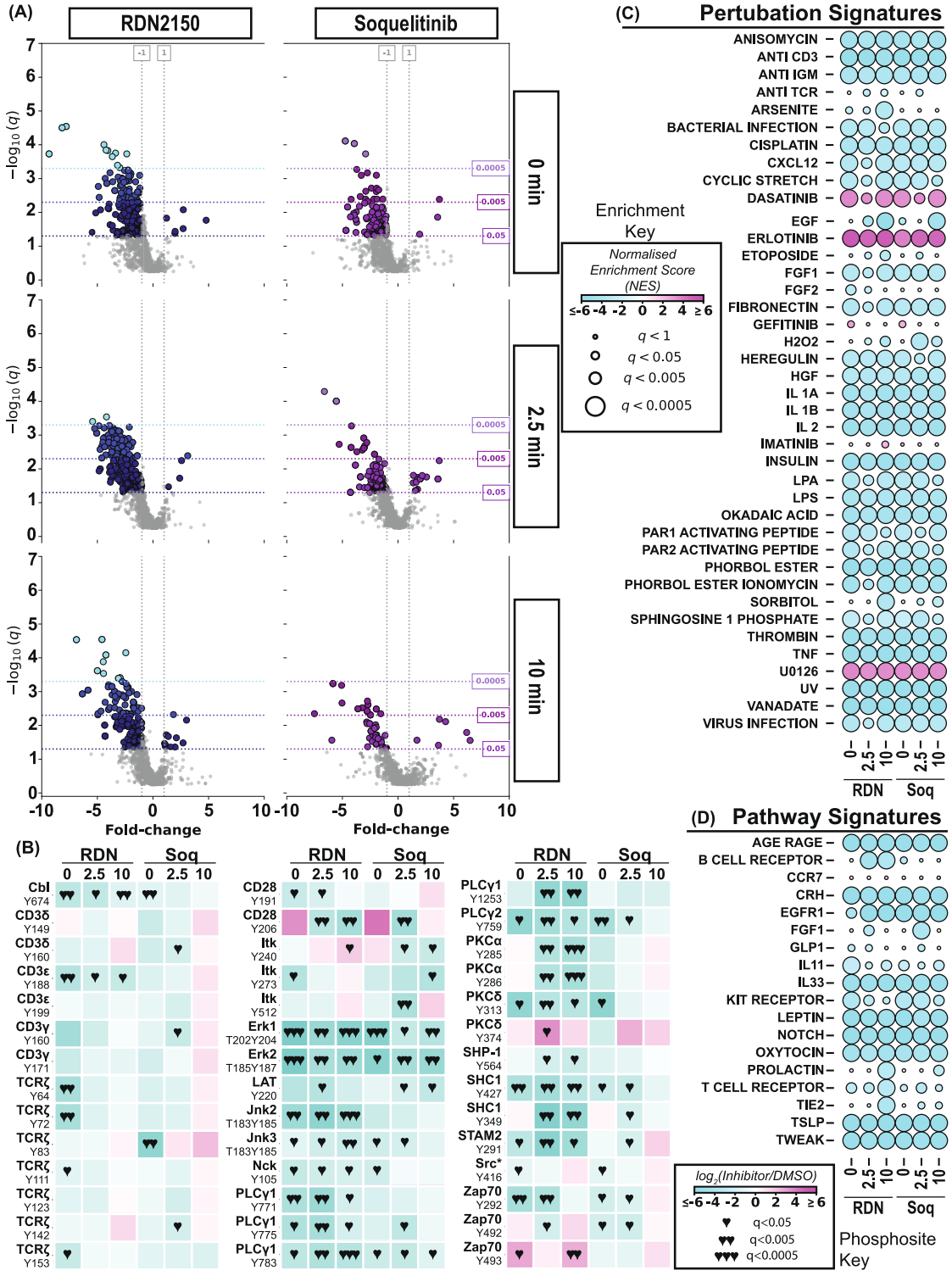

Fig. 4. 10 uM RDN treatment downregulates global pY abundance and the TCR signalling pathway more than Soq treatment. (**A**) Volcano plot analysis of pY proteomics data comparing RDN and Soq treatment to a DMSO control in samples stimulated with soluble antibodies for 0 (top row), 2.5 (middle row), and 10 (bottom row) minutes. (**B**) Heat maps comparing RDN and Soq treatment to a DMSO control for specific pY sites in the T cell signalling pathway. ♥ indicates q < 0.05, and ♥♥ indicates q < 0.005, and ♥♥♥ indicates q < 0.0005. (**C**, **D**) PTM-SEA analysis of phosphoproteomic data showing PhosphoSitePlus Perturbation Signatures and NetPath Pathway Signatures, respectively. $n \geq 3$ measurements from independent experiments for each unique pY site per treatment group/time point/stimulation method.

inhibitor treatment (Supporting Figs. 13C,D, 14C,D). In contrast, pY site abundance changes during Soq treatment were more evenly distributed in APC-pMHC/TCR and CD19-CAR/Raji co-cultures, with very few TCR signalling proteins showing reduced pY site abundance (Supporting Figs. 13, 14). Importantly, we consistently observed PLCγ1^{Y783} to be significantly reduced relative to the DMSO control in APC-pMHC/TCR and CD19-CAR/Raji co-cultures (Supporting Figs. 9, 11, 13, 14), indicating that Soq and RDN were present and active. Together, these data suggest that RDN, more than Soq, reduces pY abundance in T cells across stimulation methods.

Stimulation method-dependent effects on pY abundance during RDN and Soq treatment

Considering that RDN and Soq both significantly reduced pY abundance on T cell signalling proteins (Fig. 4, Supporting Figs. 13, 14), yet had different effects on CD69 expression and IL-2 secretion (Fig. 2), we sought to characterise the broader impact of RDN and Soq treatment. Treatment with RDN led to the greatest number of significant differentially expressed pY sites ($q < 0.05$ compared to DMSO control) at all time points in our soluble antibody stimulation model (219 vs 118, 277 vs 137, 174 vs 48 for 0-min, 2.5-min, and 10-min, respectively). Most of those sites were unique to RDN treatment (Fig. 5A–C). This trend held for APC-pMHC/TCR (Figs. 5D–F) and CD19-CAR/Raji (Fig. 5G,H) stimulations, particularly post-stimulation. Fewer than 50% of differential pY sites identified in RDN treatment were shared with Soq treatment (except at 0 min of antibody stimulation; Fig. 5A–I). These data suggest that, despite similar trends of pY abundance in TCR signalling proteins compared with the DMSO control (Fig. 4, Supporting Figs. 13, 14), RDN and Soq control unique subsets of pY sites in Jurkat T cells. In soluble antibody stimulation samples, we observed differential, non-canonical pY sites on key TCR signalling proteins, which were significantly reduced in both RDN and Soq, such as Lck^{Y470} and Fyb^{Y803}. Some TCR pY sites were significantly reduced only in RDN-treated samples, such as Cofilin-1^{Y85}, PAG^{Y317}, PAG^{Y387}, SHP-1^{Y536}, and Zap70^{Y164}, whereas others, including Itk^{Y588}, were significantly reduced during Soq treatment. Notably, we observed that pY sites on heterogeneous nuclear ribonucleoproteins (hnRNP) F^{Y82}, hnRNP K^{Y280}, and hnRNP H1^{Y82} were significantly reduced during RDN treatment. The hnRNP family of proteins is involved in stabilising pre-mRNA during mRNA maturation, and thus directly influences protein translation[44]. While the function of these pY sites is unknown, hnRNP F^{Y82} flanks a quasi-RNA recognition motif (RRM), hnRNP H1^{Y82} lays inside a qRRM, and hnRNP K^{Y280} is within an arginine-rich patch, which may be involved in phase separation of hnRNPs[44–48]. Similarly, many non-canonical pY sites on TCR signalling proteins were reduced more in RDN treatment than Soq treatment during APC-pMHC/TCR stimulation (Fig. 5K), and some pY sites were even increased in Soq treatment compared to the DMSO control, including Lck^{Y470}, Zap70^{Y164}, and Cofilin-1^{Y68}. Notably, the pY sites hnRNP 2H9^{Y296}, hnRNP M^{Y64}, and hnRNP A2/B1^{Y174} were significantly reduced by RDN treatment in APC-pMHC/TCR treatment. However, hnRNP K^{Y280} and hnRNP 2H9^{Y296} were significantly increased during Soq treatment (Fig. 5K). While the trends for RDN treatment reducing non-canonical pY sites on signalling proteins held for CD19-CAR/Raji co-culture, we observed an elevation of hnRNP M^{Y64} in RDN treatment and hnRNP K^{Y280} (2.5 min), hnRNP M^{Y64} (2.5 min), and hnRNP C1/C2^{Y137} (0 min) during Soq treatment (Fig. 5L). Altogether, our data confirm that Zap70 is the major regulator of main-line T cell signalling and is necessary for CAR signalling. Zap70 and Itk control unique, stimulation-dependent branches of the non-canonical T cell pY proteome.

Discussion

Activation via the T cell receptor and, more recently, chimeric antigen receptors has been extensively studied in Jurkat cells and primary T cells. Although Jurkat T cells are known to be deficient in PTEN, resulting in constitutive Itk localisation to the membrane[49], and show genetic instability across research groups[24], researchers use Jurkat T cells because they show relatively consistent activation/deactivation within a research group and are amenable to genetic modification. Consequently, many fundamental aspects of T cell signalling have translated from Jurkat T cells to primary cells. Using Jurkats and primary T cells, researchers demonstrate that the basic TCR/CAR pathway involves Lck/Fyn-mediated phosphorylation of ITAMs on CD3 and/or TCRζ, Zap70 phosphorylation, and activation. Subsequently, the production of a signalosome, including LAT/SLP76 in traditional T cells or CAR/SLP76 in CAR T cells, leads to signal diversification[1,5]. However, while T and CAR T cell signalling is well studied[1,5], many integral aspects of TCR/CAR signalling remain elusive. For example, researchers have only recently decoded the role of Zap70 in the kinetic gatekeeping of T cell activation[50,51] how Lck and Zap70 coordinate to promote LAT phosphorylation[9,10,12,17–21,52] and how the Itk substrate site GADS^{Y45} integrates CD28 costimulation with TCR stimulation[22,40]. Similarly, recent construction of optimized CARs that include unintuitive intracellular domains identified through high-throughput screens in Jurkat cells[17–21,52] and point mutations in CARs that can improve function[9,10,12] are the first steps toward bringing this promising immunotherapy to more patients. Notably, signalling studies of CARs and TCRs are often confounded by the choice of stimulation method (e.g., antibodies, reconstituted MHCs, cell-to-cell contact), making results difficult to compare and impossible to determine stimulation-method-dependent effects on activation. Together, while we have made significant advances in understanding TCR and CAR signalling, our fundamental understanding of the processes underlying T cell activation through these receptors remains limited.

Here, we leveraged the sensitivity of mass spectrometry-based phosphotyrosine proteomics to determine the roles of Zap70 and Itk kinase activity in Jurkat T and CAR Jurkat T cell activation using two novel T cell inhibitors. The first, RDN, was described by Rao et al. (2023) and shown to covalently modify Zap70^{C346}, which lies at the N-terminus of Zap70's catalytic domain. Rao et al. showed that RDN suppressed in vitro kinase activity more than 98% at concentrations of 1 μM, suppressed LAT^{Y220} phosphorylation in Jurkats at concentrations as low as 400 nM with 48 h of CD3 stimulation (albeit without replicates), and suppressed CD69, CD25, IFN-γ, and IL-17A production at concentrations between 100 and 400 nM in primary murine CD4 + T cells[22]. While our functional activation data agree, showing that 100–1000 nM is effective for suppressing CD69 and IL-2

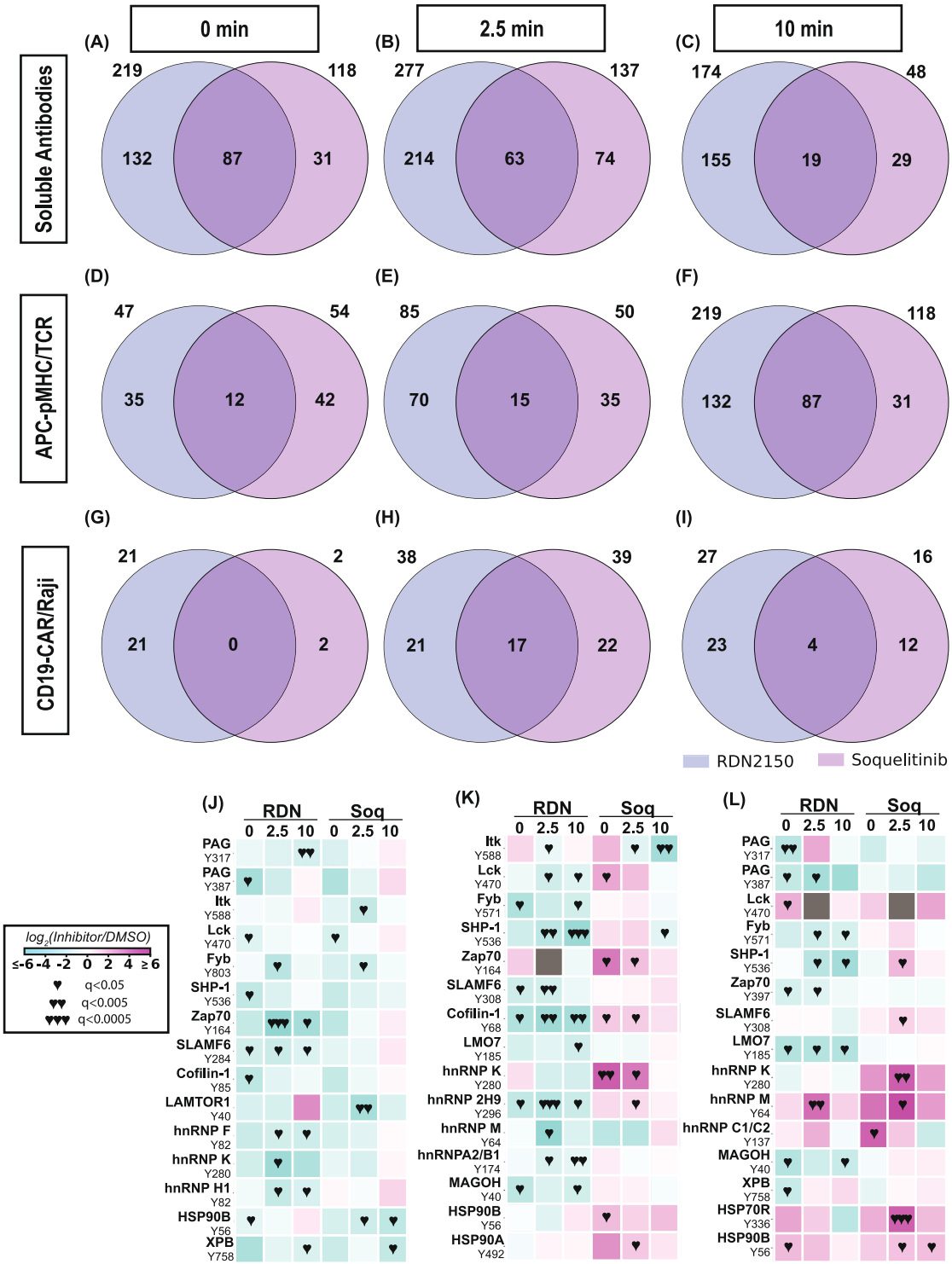

Fig. 5. Treatment with Soq increases pY abundance of non-canonical sites in response to APC-pMHC/TCR and CD19-CAR/Raji stimulation. (**A**–**C**) Venn diagrams showing overlap of unique pY sites observed as significantly changing ($q < 0.05$) compared to DMSO for soluble antibody stimulated samples at 0 min, 2.5 min, and 10 min, respectively. (**D**–**F**) As in (**A**–**C**) except for APC-pMHC/TCR stimulated samples. (**G**–**I**) As in (**A**–**C**) except for CD19-CAR/Raji stimulated samples. (**J**–**L**) Heat maps comparing RDN and Soq treatment to a DMSO control for specific, non-canonical pY sites in antibody, APC-pMHC/TCR, and CD19-CAR/Raji stimulation, respectively. ♥ indicates $q < 0.05$, and ♥♥ indicates $q < 0.005$, and ♥♥♥ indicates $q < 0.0005$. $n \geq 3$ measurements from independent experiments for each unique pY site per treatment group/time point/stimulation method.

production (Fig. 2), we found no significant decrease in LAT^{Y220} phosphorylation until 10 μM RDN after less than 20 min of CD3/CD28 crosslinking (Fig. 1), the biologically relevant timescale for LAT phosphorylation. Furthermore, we found that treatment with low concentrations of RDN could significantly enhance PLCγ1^{Y783} induction after soluble antibody stimulation (Fig. 1C) and Erk1^{T202Y204}/Erk2^{T185Y187} induction after any stimulation method (Fig. 1B; Supporting Figs. 3–5). These data are consistent with previous findings showing that the kinase domain of Zap70 mediates basal signalling and negative feedback on the TCR to ensure proper T cell signalling and activation[53,54] With a treatment of 10 μM RDN, our pY proteomics data showed that the majority of pY sites were significantly decreased when compared to a DMSO control, many of which are on integral T cell proteins like Cbl, CD28, Erk1, Erk2, LAT, Jnk2, Jnk3, Nck, PLCγ1, PKCα, PKCδ, SHP-1, SHC1, and STAM2. Further, the molecular signatures in the data resembled that of other kinase inhibitors and showed significant downregulation of signatures associated with cell signalling pathways (Fig. 4). Despite this, soluble antibody stimulation induced widespread pY in the presence of 10 μM RDN. In contrast, stimulation with APC-pMHC/TCR or CD19-CAR/Raji co-culture appeared muted in the presence or absence of RDN (Fig. 3). The residual pathway stimulation observed in the presence of either Soq or RDN (Fig. 3) could reflect partial inhibition of these kinases at the concentrations tested or the activation of compensatory pathways via parallel kinases such as Lck or Fyn. Together, these data in Jurkat cells support a model by which Zap70 is a primary driver of pY signalling from the TCR, is more effective in systems with weaker pY induction, and inhibits the production of activation markers even when insufficient to block pY signalling completely (Fig. 6), in line with the current model where Zap70 acts as a kinetic proofreader of TCR signalling.

Next, we evaluated the Itk inhibitor Soquelitinib (Soq; formerly CPI-818), developed by Corvus Pharmaceuticals and in clinical trials for T cell lymphoma treatment[55]. Recently, Hsu et al. (2024) described the synthesis and characterisation of Soq, which covalently modifies Itk^{C442}, a residue at the heart of the Itk kinase domain. Hyu et al. showed that Itk prevented CD3ε-induced PLCγ1^{Y783} phosphorylation at concentrations as low as 100 nM, impaired IL-2 production at 0.1–1 μM, significantly decreased primary cell viability at concentrations greater than 1 μM, and skewed T cell differentiation towards a Th1 phenotype[56,57]. Our data largely agreed with Hsu et al., showing that low concentrations of Soq impaired PLCγ1^{Y783} and Erk1^{T202Y204}/Erk2^{T185Y187} phosphorylation in response to CD3ε/CD28, TCR, and CAR stimulation (Fig. 1, Supporting Figs. 3–5), as well as IL-2 production (Fig. 2). Interestingly, we found that with APC-pMHC/TCR and CD19-CAR/Raji stimulation, all tested concentrations of Soq were insufficient to reduce activation-induced CD69 expression, whereas under soluble-antibody stimulation, it did significantly reduce CD69 upregulation (Fig. 2). Previous literature has shown that the kinase activity of Itk is important for IL-2 production, although the mechanism by which Itk controls IL-2 production is unclear[58], and that CD69 expression is an 'all or nothing' threshold that depends on ligand strength[53]. Thus, while our data in Jurkat cells showed that Itk is involved in CD69 production, Itk was less critical than Zap70, which was necessary for both CD69 and IL-2 production (Fig. 2). Using a treatment of 10 μM Soq, we found that global pY abundance decreased compared to a DMSO control; however, pY sites along the T cell signalling pathway did not appear to be heavily affected. Notably, PLCγ1^{Y783} and Erk1^{T202Y204}/Erk2^{T185Y187} were reduced, in line with our titration Western blot data, and some pY sites on Zap70 were significantly reduced. The molecular signatures associated with Soq treatment reflected its inhibitory activity (Fig. 4). In the context of pY induction, Soq appeared to have little effect, regardless of the stimulation method (Fig. 3A). Our data support the previously established model of Itk function, whereby Itk acts as a rheostat to tune T cell activation, with control over the IL-2 production pathway (Fig. 6).

Lastly, our data provide a comprehensive comparison of T cell activation methods frequently used in the literature, including soluble antibody stimulation of the TCR, APC-pMHC/TCR co-culture, and CD19-CAR/Raji co-culture. We found that fold induction of key TCR signalling pY sites by Western blot differed between soluble antibody, APC-pMHC/TCR, and CD19-CAR/Raji stimulations (Fig. 1), and this difference did not correlate with CD69 expression or IL-2 secretion (Fig. 2). We found that soluble antibody stimulation led to a large increase in tyrosine phosphorylation that was not seen in either APC-pMHC/TCR or CD19-CAR/Raji stimulations (Figs. 1 and 3), however, soluble antibody stimulation was unable to sufficiently promote CD69 expression or IL-2 secretion compared to APC-pMHC/TCR or CD19-CAR/Raji co-culture. While RDN and Soq reduced pY abundance on T cell signalling proteins irrespective of stimulation method (Fig. 4), they had unique effects on non-canonical TCR pY sites. In particular, RDN treatment reduced phosphorylation of multiple heterogeneous nuclear ribonucleoproteins (hnRNPs) independent of stimulation method; however, Soq treatment increased pY abundance on multiple hnRNP pY sites in APC-pMHC/TCR and CD19-CAR/Raji co-culture experiments. While many of these pY sites are uncharacterised, hnRNPs play a significant role in T cell physiology. In particular, Chang et al. (2009) showed that hnRNP K was a direct pathway target of the TCR, was required for effective IL-2 production, and promoted Vav1 proteolysis[54]. Meininger et al. (2016) showed that hnRNP U suppressed exon 7 inclusion in *MALT1* mRNA splicing, thereby regulating MALT1A expression and T cell activation[59]. White et al. showed that hnRNP L controlled differentiation of peripheral T cells, particularly into T follicular helper cells[56]. Finally, Shankarling et al. (2014) used crosslinking and immunoprecipitation sequencing to identify alternative splicing events of TCR signalling mRNAs in response to TCR signalling[57]. Although the signalling pathway linking T cell signalling and hnRNP regulation remains unclear in many cases, our data suggest that Zap70 and Itk play stimulation-dependent roles on the abundance of hnRNP pY sites.

Here, we provide a thorough, site-specific resource on the activation pathway of Jurkat T and CAR T cells in the presence of two T cell inhibitors, RDN and Soq. We confirmed that Zap70 is the dominant regulator of TCR signal initiation and T cell activation, while Itk selectively regulates IL-2 induction through a more limited branch of T cell signalling. While our studies directly inform the interpretation of high-throughput Jurkat CAR engineering screens, future targeted studies with primary human T cells will define the translational potential of these findings to improve CAR T therapies and identify the possible benefits of combination therapies.

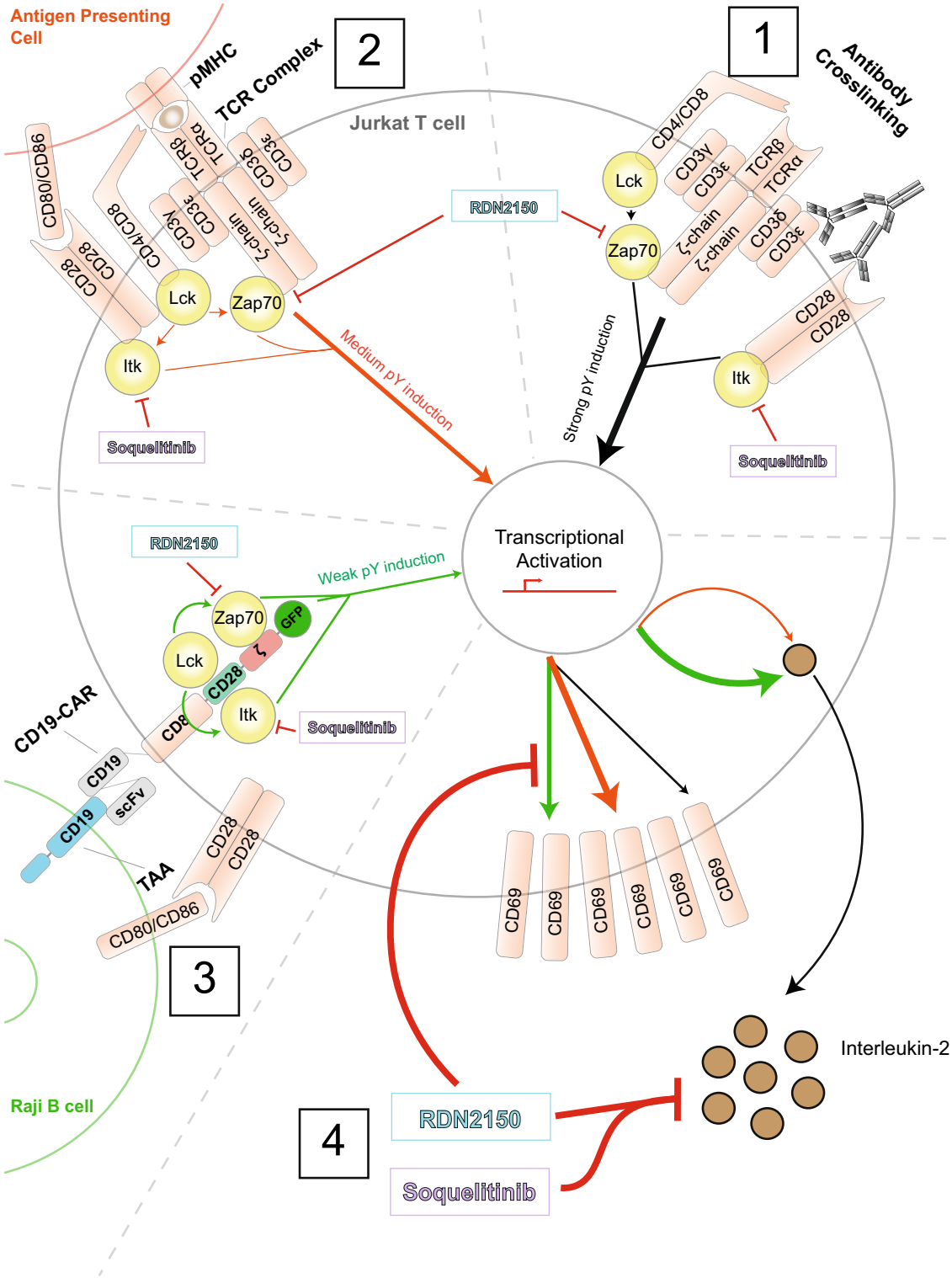

Fig. 6. pY induction and the T cell activation markers CD69/IL-2 are inversely related. [Part 1] Soluble antibody crosslinking of CD3ε and CD28 induces very strong pY signalling down the T cell signalling cascade. Treatment with RDN or Soq reduces pY abundance at 0, 2.5, and 10 min post-stimulation (Figs. 1, 3, and 4); however, pY signalling remains induced. [Part 2] CD19-CAR/Raji binding through co-culture induces TCR signalling to a milder degree than antibody crosslinking, and RDN largely impairs pY induction (Figs. 1, 4). [Part 3] CD19-CAR/Raji binding induces much weaker pY signalling than either antibody crosslinking or APC-pMHC/TCR binding. Treatment with RDN blunts pY signalling entirely (Figs. 1, 4). [Part 4] APC-pMHC/TCR and CD19-CAR/Raji co-culture induce high CD69 expression, whereas soluble antibody crosslinking does not, and soluble antibody crosslinking is unable to induce IL-2 production (Fig. 2A, C, E). RDN, but not Soq, blocks CD69 expression; however, both RDN and Soq block IL-2 production (Fig. 2).

Materials and methods

Materials

For flow cytometry, the following antibodies were used: α-CD69 APC (20 µL/2e6 T cells; BD Pharmingen #560967), α-CD45 (0.06 µg/2e6 cells; Thermo Fisher Scientific #17-0459-42) α-CD3ε PE (20 µL/2e6 T cells; BD Pharmingen #561808), α-TCRαβ PE (20 µL/2e6 T cells; BD Pharmingen #561,674), α-CD28 PE (0.25 µg/2e6 T cells; Thermo Fisher Scientific #12-0289-41), α-CD80 (0.5 µg/2e6 Raji or T2-K^b cells; Thermo Fisher Scientific #12-0809-42), α-CD86 (0.5 µg/2e6 Raji or T2-K^b cells; Thermo Fisher Scientific #12-0869-41). For Western blotting, the following antibodies were used: α-phospho-PLCγ1^{Y783} (1:2000; Cell Signaling Technologies #2821), α-phospho-LAT^{Y220} (1:2000; Cell Signaling Technologies #3584), α-phospho-SFK^{Y416} (1:2000; Cell Signaling Technologies #2101), α-phospho-Erk1^{T202Y204}/Erk2^{T185Y187} (1:2000; Cell Signaling Technologies #9101), α-PLCγ1 (1:10000; Millipore Sigma #05-163), α-LAT (1:1000; Thermo Fisher Scientific #MA1-19,307), α-Lck (1:5000; Cell Signaling Technologies #2657), α-Erk1 (1:2000; Cell Signaling Technologies #9107), IRDye 680RD Goat α-Mouse IgG (1:20000; LI-COR #926-68070), IRDye 800CW Goat α-Mouse IgG (1:20,000; LI-COR #926-33210), IRDye 680RD Donkey α-Rabbit IgG (1:20000; LI-COR #926–68,073), IRDye 800CW Donkey α-Rabbit IgG (1:20000; LI-COR #926-32213).

Cell culture and SILAC labelling

Jurkat T cells (clone E6.1), J^{OT1} (Jurkat T cells clone E6.1 expressing murine OT1 TCR, human CD8, and cytosolic GFP; gift from Dr. Arthur Weiss), 28ζ-CAR (Jurkat T cells clone E6.1 expressing a FMC63 scFv, CD8 hinge/transmembrane, CD28 costimulatory domain, TCRζ stimulation domain containing CAR with a terminal superfold GFP tag. In the J^{OT1} system, CD8/MHC recognition is present because the human CD8 expressed by J^{OT1} functionally engages murine MHC class I (H-2Kb) on T2-K^b antigen-presenting cells[50,60]. Characterised in Callahan et al. (2025)), T2-K^b cells (T2 cells expressing the Kb class 1 MHC; gift from Dr. Arthur Weiss), and Raji B cells (gift from Dr. Xiaolei Su), were maintained in RPMI 1640 supplemented with 10% FBS (Peak Serum #PS-FB3 Lot 01Z2233), 1X penicillin streptomycin glutamine (Cytiva #SV30082.01), and 2.5 µg/mL plasmocin (InvivoGen #ant-mpp) in a humidified incubator at 37 C, 5% CO_2. For co-culture phosphoproteomics, Jurkat T cell derivatives were grown initially in supplemented RPMI 1640 as described above, before transitioning to SILAC RPMI (Thermo #A33823) supplemented with 10% dialysed FBS, 1X penicillin streptomycin glutamine, and 2.5 µg/mL plasmocin, 0.38 mM $^{13}C_6$ $^{15}N_4$ Arginine (Millipore #608033), and 0.22 mM $^{13}C_6$ $^{15}N_2$ Lysine (Cambridge Isotopes #CNLM-291-H-1) for at least 7 days, as previously described[36,37].

Inhibitor treatment

For inhibitor treatment experiments, Jurkat T cells were collected by centrifugation at 400 xg for 5 min, washed once in unsupplemented RPMI 1640 (or SILAC RPMI 1640 for phosphoproteomics), then resuspended at a concentration of 1×10^7 cells/mL in RPMI 1640 supplemented with the indicated concentration of RDN (MedChemExpress #HY-155978), Soq (MedChemExpress #HY-150298), or DMSO and were allowed to incubate at 37 C, 5% CO2 in a humidified incubator for 3 h. After inhibitor treatment, the cells were collected and washed using 1X DPBS supplemented with inhibitor, then resuspended at a concentration of 2×10^8 cells/mL for stimulation.

T cell receptor/chimeric antigen receptor stimulation

Soluble antibody stimulation of the T cell receptor was performed as previously described[34]. Briefly, Jurkat T cells were suspended in RPMI 1640 at a concentration of 2×10^8 cells/mL (1×10^8 cells for pY proteomics, 1×10^7 cells for Western samples), then allowed to rest at 37 C for 30 min. T cell receptor stimulation was initiated by addition of a stimulating antibody solution (25 µL for Western, 250 µL for pY proteomics) containing α-CD3ε (Thermo #16–0037-85, clone OKT3; 2 µg/mL final concentration) and α-CD28 (Thermo #16–0288-81, clone CD28.6; 2 µg/mL final concentration) for 30 s, followed by addition of α-Mouse IgG (Jackson ImmunoResearch #115–005-062, 22 µg/mL final concentration, 25 µL for Western, 250 µL for pY proteomics). Stimulation was stopped by the addition of 9 M Urea Lysis Buffer (9 M Urea, 1 mM sodium orthovanadate, 1 mM sodium pyrophosphate, 1 mM β-glycerophosphate in 20 mM HEPES) at the indicated time point.

Co-culture stimulation of Jurkats expressing the OT1 TCR was performed by loading T2-K^b cells with OVA$^{257-264}$ (SIINFEKL; Rockland #000-001-M45) by incubation T2-K^b cells in plain RPMI 1640 supplemented with 1 µM OVA$^{257-264}$ peptide for 3 h, then washing with 1X DPBS and resuspending at 200,000,000 cells/mL (1×10^8 cells for pY proteomics, 1×10^7 cells for Western samples). Stimulation was initiated by the 1:1 (v/v) addition of OVA$^{257-264}$ loaded T2-K^b cells to J^{OT1} cells (1×10^8 cells for pY proteomics, 1×10^7 cells for Western samples) followed by a 30-s centrifugation at 500 xg to initiate cell-to-cell contact. Stimulation was stopped at the indicated time points by addition of 9 M Urea lysis buffer.

Co-culture stimulation of 28ζ-CAR T cells was performed as previously described[35,37] by 1:1 addition of Raji B cells to 28ζ-CAR T cells (1×10^8 of each cell for pY proteomics, 1×10^7 of each cell for Western samples), centrifugation at 500 xg for 30 s, and lysis with 9 M Urea Lysis Buffer. Samples for Western blotting were then sonicated and diluted 1:1 in 2 × Laemmli sample buffer, as previously described[34].

Flow cytometry

Assessment of GFP or surface expression using flow cytometry was performed by collecting 2×10^6 cells by centrifugation (400 *xg*, 5 min) from log-phase growth, resuspending cells in 100 µL of ice cold flow buffer (2% FBS in 1 × DPBS), then treating cells with fluor-conjugated antibodies for 30 min at 4 °C (or no antibody for GFP samples). Cells were washed 3 times with 1 mL of ice-cold flow buffer (centrifugation at 400 × *g*, 5 min), then resuspended in 100 µL of ice-cold flow buffer. Cells were fixed via addition of 100 µL of ice cold 4% paraformaldehyde and incubated at room temperature in the dark for 15 min. After fixing, cells were washed

3 times in 1 mL of ice-cold flow buffer (centrifugation at 1000 × *g*, 2 min). After the final wash, cells were resuspended in 100 µL of ice-cold flow buffer and stored at 4 °C in the dark until acquisition on a Cytek Aurora flow cytometer. Output files were analysed using Floreada.io, a free online tool for flow cytometry analysis, as previously described[34,35].

T cell activation was assessed by measuring surface expression of CD69 after TCR stimulation, as previously described[35]. Briefly, cells were treated with the inhibitor as described in the "Inhibitor treatment" section, except for one hour, then activated as described in the "T cell receptor/chimeric antigen receptor stimulation" section using soluble antibodies or PFA fixed target cells, then incubated at 37 °C, 5% CO_2 in 1.5 mL of complete RPMI containing inhibitor in a 6-well plate at a concentration of 7×10^5 cells/mL in a humidified incubator for 24 h. After 24 h, about 1×10^6 T cells (2×10^6 total cells) were collected by centrifugation at 400 × *g* for 5 min, then resuspended in flow cytometry buffer and treated with APC-conjugated α-CD69 antibody for 30 min at 4 °C. After flow antibody binding, cells were washed 3 times in 1 mL flow cytometry buffer, fixed with 2% PFA for 15 min in the dark, then washed 3 times in 1 mL flow cytometry buffer before analysis on a Cytek Aurora flow cytometer. Output files were analysed using Floreada.io. T cells were determined by first gating on high GFP expression, then determining CD69 positivity (Supporting Fig. 15). Statistical analysis was performed by first using an ANOVA to determine if any groups were significantly different, then using Fisher's least significant difference with the Holm-Sidak FWER correction to determine which groups were significantly different. Samples represent individual stimulation experiments, and each sample was only measured once. The cell culture supernatant from these experiments was saved and assessed for IL-2 by ELISA.

Western blotting

Western blotting was performed as previously described[34–37]. Briefly, 15 µL of lysates were separated on 10% polyacrylamide gels poured in house at 100 V for 120 min, then transferred to PVDF membranes (Millipore #IPFL00010) at 100 V for 100 min in a Wet Transfer apparatus using Tris–Glycine running and transfer buffers. Membranes were blocked in Intercept TBS Blocking Buffer (LI-COR #927-60003) for 1 h at room temperature then incubated with primary antibodies diluted in 5% BSA in 1 × TBST overnight at 4 °C. Primary antibodies solution was removed, the membranes were washed three times with 1 × TBST, then incubated with secondary antibodies diluted in 5% BSA in 1 × TBST for 1 h at room temperature. After secondary incubation, the membranes were washed three times with 1 × TBST, once with 1 × TBS, then imaged on a LI-COR OdysseyM imager. Quantification of Western blots was performed as previously described[36,37], by first correcting the signal in the phosphorylation channel using the total protein as a control, then calculating 'Fold-change' by dividing all corrected intensity values by the mean of the 0 min samples for that inhibitor treatment group. Therefore, all treatment groups start at a fold change of 0, and the observed changes are relative to the basal state for each group. Statistical analysis was performed as described in the "Flow cytometry" section. Samples represent individual stimulation experiments, and each sample was only measured once. The complete, uncropped Western blots for Fig. 1B, E, and H are provided as Supporting Figs. 16–18. All uncropped Western blots presented in Supporting Figures are presented as Supporting Figs. 19–26 with labels indicating the emission wavelength of the fluorophore conjugated to the secondary antibody, the primary antibodies used for each membrane, and lines indicating which bands correspond to which protein/phospho-protein. Labels above each membrane indicate the time point, treatment, and replicate number for the lanes on the blot from left to right.

Interleukin-2 ELISA

Samples for IL-2 ELISAs were taken from the cell culture supernatant produced during flow cytometry preparation and frozen at − 80 °C until use. Interleuken-2 abundance was assessed using the Human IL-2 Sandwich ELISA Kit (proteintech #KE00017) per the manufacturer's instructions. Briefly, 100 uL of samples diluted 1:4 in complete growth media were incubated in the ELISA plate for 2 h at room temperature and washed four times in Wash Buffer before addition of 100 uL Detection Antibody solution. The plate was incubated at room temperature for 1 h with Detection Antibody Solution, then washed four times with Wash Buffer. Next, 100 uL of Streptavidin-HRP solution was added to each well and incubated at room temperature for 40 min before washing four times with Wash Buffer. For signal development, 100 uL of TMB was added to each well and incubated for 15 min before quenching with 100 uL of Stop Solution. Absorbance was read at 450 nm with correction at 630 nm. Absolute quantitation was determined by using a standard curve of Human IL-2. Statistical analysis was performed as described in the "Flow cytometry" section. Samples represent individual stimulation experiments and each sample was only measured once.

Sample preparation and phosphoproteomic sample acquisition

Reduction, alkylation, trypsinization and desalting

Eleven milligrams of total protein were taken for each sample, then samples were adjusted to an equivalent volume (4.45 mL, ~ 1.6 M Urea final) with 20 mM HEPES, then reduced with 10 mM dithiothreitol (final) for 30 min at 37 C, then alkylated with 10 mM iodoacetamide (final) for 15 min in the dark. In solution trypsinisation was initiated with the addition of Sequencing Grade Trypsin (Promega #V5113) at a ratio of 1:100 trypsin:protein. After trypsinisation, samples were acidified to 1% trifluoroacetic acid (TFA), then cleared by centrifugation. Samples were desalted using Waters C18 vacuum columns as previously described[34]. Under low vacuum, columns were activated using 100% acetonitrile (ACN), then equilibrated with 2 washes of 0.1% TFA. Samples were then passed through the columns, trapping peptides, and washed three times with 1, 5, and 6 mL of 0.1% TFA, before elution with 40% TFA and 0.1% ACN. After elution, 10 pmol of a phosphotyrosine standard (LIEDpYTAK) was added to each sample, then each sample was diluted to 20% ACN before freezing and 48-h lyophilisation.

pY enrichment with Src SH2 superbinder

Phosphotyrosine enrichment using recombinant Src SH2 superbinder (sSH2) was performed as previously described[33–37]. Briefly, ~ 11 mg of dried peptide was resuspended in ice-cold IAP buffer (10 mM sodium phosphate monobasic monohydrate, 50 mM sodium chloride, 50 mM morpholinopropanesulfonic acid) at room temperature for 30 min with brief, interspersed vortexing. One hundred micrograms of sSH2 conjugated to agarose beads was aliquoted into microcentrifuge tubes, then washed 3 times (1500 × *g*, 2 min to collect beads) with 1 mL of ice-cold IAP buffer before addition of sample for 2 h at 4 °C on an end-over-end rotator. After pY peptide binding, beads were washed 2 times with 1 mL ice-cold IAP buffer, then 3 times with ice-cold HPLC water. After the final water wash, all liquid was removed from the beads using an insulin syringe. Phosphotyrosine peptides were eluted from the beads using 0.15% TFA on a thermomixer at 1150 rpm for 10 min, twice. Eluted pY peptides were then desalted using Empore C18 StageTips as previously described[34] and dried by speed-vac before LC–MS/MS acquisition.

LC–MS/MS acquisition

Samples were separated as previously described[34,35] on a Vanquish Neo uHPLC system with an Acclaim PepMap C18 Trap column (7 cm, 2 cm bed length, 3 µm particle size, 100 A) and IonOpticks Aurora Ultimate (25 cm long × 75 µm ID, 1.7 µm particle size) and acquired on an Orbitrap Ascend mass spectrometer (Thermo Fisher). The separation gradient started at 5% Solvent B (80% ACN, 0.1% Formic Acid [FA])/95% Solvent A (0.1% FA) and increased to 30% Solvent B over 50 min, then spiked to 99% Solvent B for the remaining 5 min of acquisition. After acquisition, the flow path was washed with 4 alternating zebra washes, alternating between 100% Solvent A and 100% Solvent B, before being reequilibrated for the next run. The spray voltage was 2050 V, the ion transfer tube temperature was 275 °C, and the lock mass was 445.12003. For MS1 acquisition, wide quant isolation on the Orbitrap detector at a resolution of 120,000 with a mass range of 300–1500 m/z was used. The maximum injection time was 50 ms, the normalised AGC target was 250%, and the RF lens was set to 30%, and data collection was in centroid mode. The following filters were included: monoisotopic peak and peptide mode, Charge state (+2 to +7), Precursor Selection Range (375–1500 m/z), Dynamic Exclusion (exclude after 1 time, 15 s exclusion time, 10 ppm low and high mass tolerance, excluding isotopes), Intensity Threshold (intensity range of 20,000 (min) – 1E20 (max) with relative intensity threshold of 20%). MS2 spectra were acquired in data-dependent mode with a cycle time of 3 s, normalised HCD fragmentation energy of 30%, and a 0.7 m/s quadrupole isolation window. Peptide fragments were detected using the ion trap detector with Turbo Mode active (scan range 150–2000 m/z) in centroid mode with the following settings: 35 ms maximum injection time, 100% normalised AGC target, dynamic maximum injection time active.

Data analysis, database searching and relative abundance quantification

RAW files from the mass spectrometer were searched as previously described using the High Throughput Autonomous Proteomics Pipeline[61] and PeptideDepot[62]. MS2 spectra were searched using the Mascot search engine against the complete UniProt proteome dataset (downloaded August 2019, 98,300 unique forward sequences) with a 0.1% FDR cutoff against a decoy database. The following parameters were used for peptide spectrum matching: trypsin (up to 2 missed cleavages), precursor mass tolerance of 7 ppm, 500 mmu fragment ion mass tolerance, phosphorylation as a variable modification (S/T/Y + 79.9963 Da), oxidation as a variable modification (M + 15.9949), and SILAC labelling (K: + 8.0142 Da, R: + 10.0083 Da) and carbamidomethylation (C + 57.0215) as a static modification. Relative peptide abundance was determined using peak area integration and retention time alignment of selected ion chromatograms. The abundance of pY peptides was normalised using the spike in standard peptide LIEDpYTAK, and any samples without LIEDpYTAK identified were omitted. Statistical significance between the log2 mean abundance for each comparison was determined using Welch's T test and corrected using the method of Storey[63] as previously described. Post-translational modification signature enrichment analysis was performed as previously described[41].

All post-PeptideDepot data processing was performed using Python 3.10 in the Windows Subsystem for Linux 2 in JupyterLab environments with the following dependencies: matplotlib (3.10.1), scipy (1.15.2), numpy (2.2.5), scikitlearn (1.6.1), pandas (2.2.3), and a custom 'helpers' module for improving matplotlib graph quality. The Holm Sidak algorithm for FWER correction was performed using a self-coded version of the algorithm as described by GraphPad Prism. All code used for the analysis of the data are publicly available on GitHub (https://github.com/Aurdeegz/Zap70-Itk-Inhibitor-Profiling).

Data availability

All uncropped LICOR full Western blot images, Floreada workspaces, and all code used for the analysis and presentation of our mass spectrometry data are publicly available on GitHub (https://github.com/Aurdeegz/Zap70-Itk-Inhibitor-Profiling). Mass spectrometry data are available from the ProteomeXchange Consortium via the PRIDE repository (Dataset ID: PXD069485).

Received: 4 November 2025; Accepted: 30 March 2026
Published online: 06 April 2026

References

1. Gaud, G., Lesourne, R. & Love, P. E. Regulatory mechanisms in T cell receptor signalling. *Nat. Rev. Immunol.* **18**, 485–497 (2018).
2. Weeks, S., Harris, R. & Karimi, M. Targeting ITK signaling for T cell-mediated diseases. *iScience* **24**, 102842 (2021).
3. Au-Yeung, B. B., Shah, N. H., Shen, L. & Weiss, A. ZAP-70 in signaling, biology, and disease. *Annu. Rev. Immunol.* **36**, 127–156 (2018).

4. Labanieh, L. & Mackall, C. L. CAR immune cells: Design principles, resistance and the next generation. *Nature* **614**, 635–648 (2023).
5. Lindner, S. E., Johnson, S. M., Brown, C. E. & Wang, L. D. Chimeric antigen receptor signaling: Functional consequences and design implications. *Sci. Adv.* **6**, eaaz3223 (2020).
6. Sengsayadeth, S., Savani, B. N., Oluwole, O. & Dholaria, B. Overview of approved CAR-T therapies, ongoing clinical trials, and its impact on clinical practice. *eJHaem* **3**, 6–10 (2022).
7. Srivastava, S. & Riddell, S. R. Engineering CAR-T cells: Design concepts. *Trends Immunol.* **36**, 494–502 (2015).
8. Zhang, Y. et al. Exploring CAR-T cell therapy side effects: Mechanisms and management strategies. *J. Clin. Med.* **12**, 6124 (2023).
9. Salter, A. I. et al. Phosphoproteomic analysis of chimeric antigen receptor signaling reveals kinetic and quantitative differences that affect cell function. *Sci. Signal.* **11**, eaat6753 (2018).
10. Salter, A. I. et al. Comparative analysis of TCR and CAR signaling informs CAR designs with superior antigen sensitivity and in vivo function. *Sci. Signal.* **14**, eabe2606 (2021).
11. Philipson, B. I. et al. 4-1BB costimulation promotes CAR T cell survival through noncanonical NF-κB signaling. *Sci. Signal.* **13**, eaay8248 (2020).
12. Boucher, J. C. et al. CD28 costimulatory domain–targeted mutations enhance chimeric antigen receptor T-cell function. *Cancer Immunol. Res.* **9**, 62–74 (2021).
13. Guedan, S. et al. Single residue in CD28-costimulated CAR-T cells limits long-term persistence and antitumor durability. *J. Clin. Investig.* **130**, 3087–3097 (2020).
14. Chmielewski, M. & Abken, H. TRUCKS, the fourth-generation CAR T cells: Current developments and clinical translation. *Adv. Cell Gene Ther.* **3**, e84 (2020).
15. Tousley, A. M. et al. Co-opting signalling molecules enables logic-gated control of CAR T cells. *Nature* **615**, 507–516 (2023).
16. He, X. et al. Bispecific and split CAR T cells targeting CD13 and TIM3 eradicate acute myeloid leukemia. *Blood* **135**, 713–723 (2020).
17. Goodman, D. B. et al. Pooled screening of CAR T cells identifies diverse immune signaling domains for next-generation immunotherapies. *Sci. Transl. Med.* **14**, eabm1463 (2022).
18. Gordon, K. S. et al. Pooled screening for CAR function identifies novel IL-13Rα2-targeted CARs for treatment of glioblastoma. *J. Immunother. Cancer* **13**, e009574 (2025).
19. Gordon, K. S. et al. Screening for CD19-specific chimaeric antigen receptors with enhanced signalling via a barcoded library of intracellular domains. *Nat. Biomed. Eng.* **6**, 855–866 (2022).
20. Kang, C. H. et al. Identification of potent CD19 scFv for CAR T cells through scFv screening with NK/T-cell line. *Int. J. Mol. Sci.* **21**, 9163 (2020).
21. Rydzek, J. et al. Chimeric antigen receptor library screening using a novel NF-κB/NFAT reporter cell platform. *Mol. Ther.* **27**, 287–299 (2019).
22. Rao, D. et al. Discovery and structural optimization of covalent ZAP-70 kinase inhibitors against psoriasis. *J. Med. Chem.* **66**, 12018–12032 (2023).
23. Hsu, L.-Y. et al. Synthesis and characterization of soquelitinib a selective ITK inhibitor that modulates tumor immunity. *npj Drug Discov.* **1**, 2 (2024).
24. Wilson, A. et al. Jurkat T-cell lines exhibit marked genomic instability affecting karyotype, mutational profile, gene expression, immunophenotype and function. *Sci. Rep.* **15**, 22426 (2025).
25. Abraham, R. T. & Weiss, A. Jurkat T cells and development of the T-cell receptor signalling paradigm. *Nat. Rev. Immunol.* **4**, 301–308 (2004).
26. Paz, P. E. et al. Mapping the Zap-70 phosphorylation sites on LAT (linker for activation of T cells) required for recruitment and activation of signalling proteins in T cells. *Biochem. J.* **356**, 461–471 (2001).
27. Moulton, V. R. & Tsokos, G. C. T cell signaling abnormalities contribute to aberrant immune cell function and autoimmunity. *J. Clin. Invest.* **125**, 2220–2227 (2015).
28. Geppert, T. D. & Lipsky, P. E. Activation of T lymphocytes by immobilized monoclonal antibodies to CD3. Regulatory influences of monoclonal antibodies to additional T cell surface determinants. *J. Clin. Investig.* **81**, 1497–1505 (1988).
29. Hu, K. H. & Butte, M. J. T cell activation requires force generation. *J. Cell Biol.* **213**, 535–542 (2016).
30. Fritzsche, M. & Kruse, K. Mechanical force matters in early T cell activation. *Proc. Natl. Acad. Sci. U.S.A.* **121**, e2404748121 (2024).
31. Trickett, A. & Kwan, Y. L. T cell stimulation and expansion using anti-CD3/CD28 beads. *J. Immunol. Methods* **275**, 251–255 (2003).
32. Manger, B., Weiss, A., Imboden, J., Laing, T. & Stobo, J. D. The role of protein kinase C in transmembrane signaling by the T cell antigen receptor complex. Effects of stimulation with soluble or immobilized CD3 antibodies. *J. Immunol.* **139**, 2755–2760 (1987).
33. Callahan, A. et al. Deep phosphotyrosine characterisation of primary murine T cells using broad spectrum optimisation of selective triggering. *PROTEOMICS* **24**, 2400106 (2024).
34. Callahan, A., Mojumdar, A., Salomon, A. R. & DaSilva, N. A. Evaluating first-pass, high protein capacity desalting techniques for phosphoproteomics applications. *bioRxiv*, 2025.2006.2003.657744, (2025).
35. Callahan, A. et al. Phosphoproteomic analysis of successive Jurkat CD19-CAR generations reveals TCRζ-driven signalling. *Cell. Signal.* **138**, 112204 (2026).
36. Griffith, A. A. et al. SILAC phosphoproteomics reveals unique signaling circuits in CAR-T cells and the inhibition of B cell-activating phosphorylation in target cells. *J. Proteome Res.* **21**, 395–409 (2022).
37. Callahan, A. et al. CSF1R-CAR T cells induce CSF1R signaling and can promote target cell proliferation. *Sci. Signal.* **18**, eadv4112 (2025).
38. Belmont, J., Gu, T., Mudd, A. & Salomon, A. R. A PLC-γ1 feedback pathway regulates Lck substrate phosphorylation at the T-cell receptor and SLP-76 complex. *J. Proteome Res.* **16**, 2729–2742 (2017).
39. Helou, Y. A., Nguyen, V., Beik, S. P. & Salomon, A. R. ERK positive feedback regulates a widespread network of tyrosine phosphorylation sites across canonical T cell signaling and actin cytoskeletal proteins in Jurkat T cells. *PLoS ONE* **8**, e69641 (2013).
40. Sjölin-Goodfellow, H. et al. The catalytic activity of the kinase ZAP-70 mediates basal signaling and negative feedback of the T cell receptor pathway. *Sci. Signal.* **8**, ra49–ra49 (2015).
41. Krug, K. et al. A curated resource for phosphosite-specific signature analysis. *Mol. Cell. Proteomics* **18**, 576–593 (2019).
42. Gudipati, V. et al. Inefficient ZAP70-signaling blunts antigen detection by CAR-T-cells. *bioRxiv*, 720417 (2019).
43. Chu, G. J. et al. The 4-1BBζ costimulatory domain in chimeric antigen receptors enhances CD8+ T-cell functionality following T-cell receptor stimulation. *Cancer Cell Int.* **23**, 327 (2023).
44. Geuens, T., Bouhy, D. & Timmerman, V. The hnRNP family: Insights into their role in health and disease. *Hum. Genet.* **135**, 851–867 (2016).
45. Martin, E. W. et al. Interplay of folded domains and the disordered low-complexity domain in mediating hnRNPA1 phase separation. *Nucleic Acids Res.* **49**, 2931–2945 (2021).
46. Lorton, B. M. & Shechter, D. Cellular consequences of arginine methylation. *Cell. Mol. Life Sci.* **76**, 2933–2956 (2019).
47. Moritz, B. et al. Biophysical and biochemical analysis of hnRNP K: Arginine methylation, reversible aggregation and combinatorial binding to nucleic acids. *Biol. Chem.* **395**, 837–853 (2014).
48. Ryan, V. H. et al. Mechanistic view of hnRNPA2 low-complexity domain structure, interactions, and phase separation altered by mutation and arginine methylation. *Mol. Cell* **69**, 465-479.e467 (2018).

49. Shan, X. et al. Deficiency of PTEN in Jurkat T cells causes constitutive localization of Itk to the plasma membrane and hyperresponsiveness to CD3 stimulation. *Mol. Cell. Biol.* **20**, 6945–6957 (2000).
50. Lo, W.-L. et al. Lck promotes Zap70-dependent LAT phosphorylation by bridging Zap70 to LAT. *Nat. Immunol.* **19**, 733–741 (2018).
51. Hallumi, E. et al. Itk promotes the integration of TCR and CD28 costimulation through its direct substrates SLP-76 and Gads. *J. Immunol.* **206**, 2322–2337 (2021).
52. Zhang, C. et al. Screening and characterization of the scFv for chimeric antigen receptor T cells targeting CEA-positive carcinoma. *Front. Immunol.* https://doi.org/10.3389/fimmu.2023.1182409 (2023).
53. Conley, J. M., Gallagher, M. P., Rao, A. & Berg, L. J. Activation of the Tec kinase ITK controls graded IRF4 expression in response to variations in TCR signal strength. *J. Immunol.* **205**, 335–345 (2020).
54. Chang, J.-W., Koike, T. & Iwashima, M. hnRNP-K is a nuclear target of TCR-activated ERK and required for T-cell late activation. *Int. Immunol.* **21**, 1351–1361 (2009).
55. *Corvus Pharmaceuticals Confirms Planned Initiation of Soquelitinib (CPI-818) Phase 3 Registrational Clinical Trial in Peripheral T Cell Lymphoma Following Meeting with FDA*, 2023).
56. White, T. L. A. et al. HnRNP L is essential for peripheral T cell proliferation and survival. *Front. Immunol.* **16**, 1543145 (2025).
57. Shankarling, G., Cole, B. S., Mallory, M. J. & Lynch, K. W. Transcriptome-wide RNA interaction profiling reveals physical and functional targets of hnRNP L in human T cells. *Mol. Cell. Biol.* **34**, 71–83 (2014).
58. von Bonin, A. et al. Inhibition of the IL-2-inducible tyrosine kinase (Itk) activity: A new concept for the therapy of inflammatory skin diseases. *Exp. Dermatol.* **20**, 41–47 (2011).
59. Meininger, I. et al. Alternative splicing of MALT1 controls signalling and activation of CD4+ T cells. *Nat. Commun.* **7**, 11292 (2016).
60. Moots, R. J. et al. A cross-species functional interaction between the murine major histocompatibility complex class I alpha 3 domain and human CD8 revealed by peptide-specific cytotoxic T lymphocytes. *Eur. J. Immunol.* **22**, 1643–1646 (1992).
61. Yu, K. & Salomon, A. R. HTAPP: High-throughput autonomous proteomic pipeline. *Proteomics* **10**, 2113–2122 (2010).
62. Yu, K. & Salomon, A. R. PeptideDepot: Flexible relational database for visual analysis of quantitative proteomic data and integration of existing protein information. *Proteomics* **9**, 5350–5358 (2009).
63. Storey, J. D. & Tibshirani, R. Statistical significance for genomewide studies. *Proc. Natl. Acad. Sci. U. S. A.* **100**, 9440–9445 (2003).

Acknowledgements

The authors would like to thank Dr. Xiaolei Su and his research team for providing the Jurkat CAR T cells for these experiments, as well as the group of Dr. Arthur Weiss for providing T2-Kb cells and Jurkat cells expressing the murine OT1 TCR & CD8. We would also like to wish Dr. Weiss a happy retirement and thank him for our years of enjoyable and productive collaborations.

Author contributions

Conceptualisation: AC; Methodology: AC; Investigation: AC, SST, AM, TR; Visualisation: AC; Funding acquisition: ARS; Project administration: AC; Supervision: AC, ARS; Writing: original draft: AC; Writing: review & editing: AC, ARS.

Funding

This work was supported by NIH grants P01AI091580, T32GM136566, and 1S10OD036295.

Declarations

Competing interests

The authors declare no competing interests.

Additional information

Supplementary Information The online version contains supplementary material available at https://doi.org/10.1038/s41598-026-47234-x.

Correspondence and requests for materials should be addressed to A.R.S.